Assessment of Stimulus-Induced Changes in Human V1 Visual Field Maps

Junjie V. Liu, Hiroshi Ashida, Andrew T. Smith and Brian A. Wandell

J Neurophysiol 96:3398-3408, 2006. First published Sep 27, 2006; doi:10.1152/jn.00556.2006

J Neurophysiol 96: 3398–3408, 2006.
First published September 27, 2006; doi:10.1152/jn.00556.2006.

Assessment of Stimulus-Induced Changes in Human V1 Visual Field Maps

Junjie V. Liu,[1] Hiroshi Ashida,[2,3] Andrew T. Smith,[2] and Brian A. Wandell[4]

[1]*Departments of Applied Physics and* [4]*Psychology, Stanford University, Stanford, California;* [2]*Department of Psychology, Royal Holloway, University of London, Surrey, United Kingdom; and* [3]*Graduate School of Letters, Kyoto University, Kyoto, Japan*

Submitted 24 May 2006; accepted in final form 8 September 2006

Liu, Junjie V., Hiroshi Ashida, Andrew T. Smith, and Brian A. Wandell. Assessment of stimulus-induced changes in human V1 visual field maps. *J Neurophysiol* 96: 3398–3408, 2006. First published September 27, 2006; doi:10.1152/jn.00556.2006. Visual cortex contains a set of field maps in which nearby scene points are represented in the responses of nearby neurons. We tested a recent hypothesis that the visual field map in primary visual cortex (V1) is dynamic, changing in response to stimulus motion direction. The original experimental report replicates, but further experimental and analytical investigations do not support, the interpretation of the results. The V1 map remains invariant when measured using stimuli moving in different directions. The measurements can be explained by small and systematic response amplitude differences that arise when probing with stimuli moving in different directions.

INTRODUCTION

Primate visual cortex can be subdivided into a set of distinct regions, the neuronal receptive fields of which are arranged into visual field maps: nearby scene points are represented in the responses of nearby neurons (Allman and Kaas 1971; Kaas 1997a,b). There is a particularly clear visual field map in primary visual cortex (V1) that can be identified readily using functional MRI in both human and macaque (Brewer et al. 2002; DeYoe et al. 1996; Engel et al. 1994, 1997; Sereno et al. 1995).

The stability of visual receptive fields and maps in adult, particularly after peripheral damage, has been debated (Darian-Smith and Gilbert 1995; Gilbert 1998; Gilbert and Wiesel 1992; Horton and Hocking 1998; Rosa et al. 1995; Smirnakis et al. 2005). A current remarkable claim is that the V1 visual map, even in healthy adults, is flexible (Whitney et al. 2003). These authors suggest that the relationship between the stimulus visual field location and the position of V1 cortical response can be altered by several centimeters by changing a simple stimulus property (motion direction). In their experiments, these authors presented four static apertures arranged around fixation; each aperture contained gratings drifting either toward or away from the fixation point (inward or outward). On the assumption of a fixed retinotopic map, stimuli presented within these fixed apertures should produce blood oxygen-level-dependent (BOLD) responses at the same positions in visual cortex. But, surprisingly, contrasting the responses to two motion directions within the apertures produced a differential response in which inward and outward activations were separated by several centimeters. The authors interpreted these measurements as showing that "the retinotopic representation of a stationary object in the cortex was systematically shifted when visual motion was present in the scene" (see abstract of Whitney et al. 2003).

If visual field maps are flexible, not stable, then many principles of cortical anatomy and functional organization require re-thinking. Because of the importance of the issue, our two groups independently decided to investigate the experiments that are the basis for the claimed flexibility of the visual field map.

Whereas the basic experimental findings were successfully replicated, we included additional experimental conditions and quantitative measurements. In the first set of experiments, we contrast the spatial distribution of BOLD responses to moving stimuli within a fixed aperture with blank. We find that as stimulus motion direction changes, the spatial distribution of the BOLD responses change very little. In a second set of experiments, we measure visual field maps using stimuli with opposite motion directions (DeYoe et al. 1996; Engel et al. 1994, 1997; Sereno et al. 1995). The second experiment allowed us to assess *1*) the effect of stimulus motion direction across a wide range of eccentricities and *2*) the degree to which this putative confound might affect the widely used method for visual field mapping. Again we find that these measurements estimate nearly identical visual field maps; the differences between them, if any, are much smaller than the variance of the measurements. Finally, we describe models that do not require the assumption of flexible retinotopy and shifts of neural receptive fields that explain the data.

Taken together, our experimental results do *not* support a significant reorganization of the cortical visual field map. The findings from our groups support the same conclusions, and we report our combined work here. Parts of this work have been described in abstract form (Ashida and Smith 2005; Liu et al. 2004).

METHODS

To examine the claim that visual field maps are flexible depending on the stimulus motion direction, we measured the visual field representations using stimuli with opposite motion directions. Experiments were conducted at two sites, Royal Holloway, University of London, U.K., and Stanford University, CA. There were some differences in methods, but results from the two groups are in excellent agreement. Unless specified otherwise, all methods refer to experiments conducted at Stanford.

Three human subjects (*S1–S3*) participated at Stanford, and another six subjects (*R1–R6*) participated at Royal Holloway. All subjects (age: 20–45 yr) were healthy, had normal vision, and were screened in accordance with standard procedures; written informed consent was

Address for reprint requests and other correspondence: B. A. Wandell, Jordan Hall, Stanford University, Stanford, CA 94305 (E-mail: wandell@stanford.edu).

The costs of publication of this article were defrayed in part by the payment of page charges. The article must therefore be hereby marked "*advertisement*" in accordance with 18 U.S.C. Section 1734 solely to indicate this fact.

obtained using procedures approved by local institutional review boards.

Visual stimuli

Visual stimuli were generated using the psychophysics toolbox (http://psychtoolbox.org). Stimuli were projected onto a screen (liquid-crystal projector, 800 × 600 pixels, 60-Hz refresh rate). The viewing distance was 22 cm, and the screen subtended 40 × 30° (viewed directly). To ensure that the eye convergence at short (22 cm) viewing distance does not play a significant role, in some experiments, the stimuli were displayed onto a flat-panel liquid-crystal display and viewed through binoculars (effective viewing distance 50 cm; screen subtended 44 × 35°). Results were unchanged when using this alternative configuration. At Royal Holloway, stimuli were displayed using custom software but a similar projector configuration (1,024 × 768 pixels, 60 Hz). The screen subtended ~30° across when viewed directly or ~70° across when viewed monocularly through custom-built magnifying lens.

Fixed-aperture motion stimuli

We studied extensively the category of fixed-aperture stimuli, where visual contrast was presented only within a fixed aperture in the display that was otherwise blank (gray). Three types of stimuli were studied: "in versus blank," "out versus blank," and "in versus out." Each scan included 6.5 cycles of one type of stimulus; each cycle comprising the first block (12 s) followed by the second block (12 s). Radial sinusoidal gratings (50% contrast) moved inward within a fixed, sharply defined circular aperture during an "in" block or outward during an "out" block (Fig. 1*A*). The blank block had 0% contrast. One set of measurements used 0.66 cycle/° gratings moving at 3.75°/s within the aperture of 4.5–7.5°. Another set of measurements tested a more peripheral portion of visual field, with 0.33 cycle/° gratings moving at 7.5°/s within the aperture of 7.5–13.5°. Subjects fixated at a small fixation mark (0.2° radius) and performed a demanding task involving the mark's shape to control attention, described in (Liu and Wandell 2005).

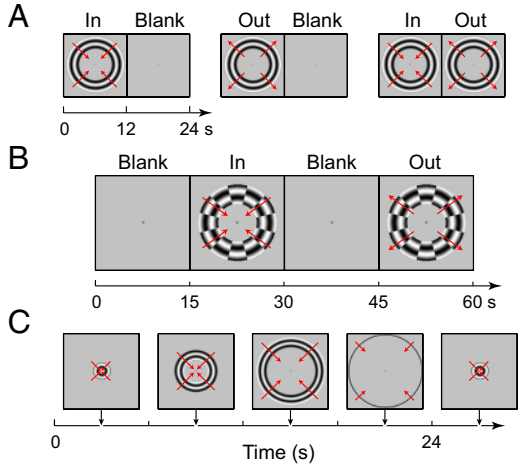

FIG. 1. Visual stimuli. *A*: 3 types of stimulus exchanges were used in the Stanford fixed-aperture measurements (in-blank, out-blank, and in-out). A cycle of each exchange type (24 s) is shown. The red arrows denote the direction of grating motion within the aperture. *B*: Royal Holloway fixed-aperture measurements in a block design; each cycle (60 s) comprised a consequence of 4 blocks: blank-in-blank-out (shown) or blank-out-blank-in. *C*: traveling wave stimulus where a pattern moving inward was within an aperture (ring) that expanded every 1 s from foveal to peripheral visual field. Stimuli at 3, 9, 15, and 21 s were illustrated. The stimulus made a complete cycle in 24 s. This is 1 of 4 types of traveling-wave measurements (expanding/contracting ring with inward/outward motion) for evaluating retinotopy reliability.

At Royal Holloway, measurements were made with similar fixed-aperture stimuli but different spatiotemporal parameters. Two types of motion stimuli (in and out) were compared with blank in a block design; each scan included eight cycles where each cycle comprised a sequence of four blocks (blank-in-blank-out or blank-out-blank-in, each block 15 s). To enhance the perception of contrast and motion, the contrasted stimuli were built by dividing a radial sinusoidal grating (80% contrast, 0.23 cycle/°) into 12 polar sectors, then shifting the spatial phase of half the sectors by π to create maximum contrast between neighboring sectors (Fig. 1*B*). The sectored gratings moving at 10.9°/s were within the fixed sharp circular aperture of 6–12°. A fixation mark was placed in the center.

Gabor patches were also tested as a control experiment at Royal Holloway to test the claim that smoothed apertures yielded similar results to the sharply defined apertures (Whitney et al. 2003). The contrasted stimuli comprised four Gabor patches in the center of 4 quadrants, all centered at 8° eccentricity with Gaussian windows of 2° SD. The carrier sinusoidal grating had the same frequency, speed, and contrast.

Traveling wave stimuli

Traveling wave stimuli present a stimulus aperture, the position of which changes over time. These stimuli are frequently used to measure visual field maps (Engel et al. 1997; Wandell et al. 2005). To evaluate the effect of stimulus motion direction on visual field maps, we measured (at Stanford only) the eccentricity maps using four types of traveling wave stimulus: expanding or contracting aperture (ring) containing a radial sinusoidal grating pattern (0.4 cycle/°; full-contrast) that moved either inward or outward (5°/s), see Fig. 1*C*. Each of the four stimulus types was measured in four pseudo-randomly ordered scans. Each scan included 6.5 cycles of one type of stimulus (24 s/cycle, 156 s total), and the first half-cycle (12 s) of data was discarded.

During each expanding ring stimulus cycle, the sharply defined aperture began as a 1° radius disk that increased every second in discrete steps of 1° until becoming a 5°-radius disk. Then the aperture became an annulus (5° width), and the outer and inner edges of the annulus continued to expand (1°/s; 1-s steps) until reaching an eccentricity of 18°. Arriving at this point, the outer edge remained fixed. The inner edge continued to expand, reducing the annulus width until finally the entire field became uniform. Then the cycle began again with the 1°-radius disk. The contracting ring cycle began with the same 1° aperture but was time-reversed from the expanding cycle.

In separate sessions, we measured the visual field maps and defined primary visual cortex (V1) using conventional ring and wedge stimuli. These stimuli were counter-balanced in motion direction to eliminate any potential effect on visual field maps. At Stanford, we used the same scan design (6.5 cycles). Ring stimuli were similar to aforementioned except that the ring was divided into 24 polar sectors where the motion directions of gratings in two neighboring sectors are always reversed against each other, and the motion direction in each sector reverses between inward and outward every 1 s. Wedge stimuli used a black-white radial dartboard pattern (0.2 cycle/°; 10°/s radial drifting speed) that was similarly divided into 24 polar sectors and motion counter-balanced. The wedge aperture (45° polar angle, 0–18° eccentricity) rotated 22.5° every 1.5 s, clockwise or counter-clockwise in different scans.

At Royal Holloway the ring stimuli comprised a high-contrast flickering (8 Hz) checkerboard pattern within a ring aperture (8° width) that expanded or contracted by 2° eccentricity every 3 s (54 s/cycle). The wedge stimulus comprised the checkerboard pattern within a wedge aperture (80° polar angle) that rotated clockwise or counter-clockwise by 20° every 3 s (54 s/cycle). (Smith et al. 1998, 2001). Each scan included five stimulus cycles (270 s). In some subjects (*R2, R5,* and *R6*), the horizontal and vertical meridians were measured using a bow-tie stimulus instead of the rotating wedge. The

bow-tie stimulus comprised the same checkerboard pattern within two opposing, bow-tie shaped apertures (45° polar angle). The apertures altered their orientation between horizontal and vertical every 15 s. All but one (*R5*) subject viewed these stimuli monocularly (right eye) through the magnifier lens; the maximum stimulated eccentricity was therefore ~35°. *Subject R5* viewed binocularly without the lens (maximum eccentricity ~15°).

Data acquisition

The data-acquisition methods at Stanford were described in detail elsewhere (Liu and Wandell 2005). Briefly, BOLD signals were acquired using a spiral T2*-weighted pulse sequence (repetition time, 1.2 s; 2 interleaves; echo time, 30 ms; flip angle, 65°; 20 slices) at a 3.0T General Electric scanner with a receive-only surface coil (Nova Medical). The effective sampling resolutions were 2.4 s and 2.5 × 2.5 × 3 mm. Slight parameter modifications were made in the traveling wave measurements (repetition time, 1.5 s; 1 interleave; flip angle, 71°; effective temporal resolution, 1.5 s).

Functional data at Royal Holloway were acquired using a 3T Siemens Trio scanner equipped with an eight-channel phased-array head coil. The head was lightly clamped to minimize head motion. BOLD signals were measured using T2*-weighted gradient-recalled echo-planar imaging (EPI) sequences and parallel imaging [GRAPPA; with acceleration factor 2 (see Griswold et al. 2002)]. Twenty coronal slices covering the occipital cortex were acquired (repetition time, 1.5 s; echo time, 31 ms; flip angle, 90°; effective spatial resolution: 2.5 × 2.5 × 2.5 mm; effective temporal resolution: 1.5 s). Slight parameter modifications (35 axial slices; repetition time and effective temporal resolution, 2.5 s) were used in the traveling wave measurements of three subjects (*R1, R3,* and *R4*).

At the beginning of each session in both data sets, we acquired a set of T1-weighted anatomical images matched in location with the functional images. In separate sessions, a few sets of T1-weighted whole-brain anatomical images were acquired, co-registered and averaged into a three-dimensional anatomical reference volume (resolution: 1 × 1 × 1 mm) for each subject.

Data analysis

At Stanford, functional data were analyzed voxel by voxel without spatial smoothing, using custom software mrVista (http://white.stanford.edu/software/). Most scans had minimal head motion and did not require motion correction. Nevertheless, we applied rigid-body motion correction in postprocessing to fixed-aperture data of *subject S2* and all traveling-wave data. In each session, the average images (mean) of functional data were compared with the anatomical images acquired at the same slice locations. In most cases, the head motion between the anatomical and functional acquisitions is negligible with respect to the low spatial resolution. Thus we co-align the anatomical images in each session with the three-dimensional (3-D) whole-brain anatomical reference volume, using a semi-automatic algorithm (Nestares and Heeger 2000). The co-alignment transformation matrix is then used to co-register functional data to the reference volume. For each subject, the reference volume was segmented into gray and white matter using custom software mrGray (http://white.stanford.edu/~brian/mri/segmentUnfold.htm). Functional data analysis was subsequently restricted to the gray matter.

Time series analysis

TWO-BLOCK DESIGN. Slow baselines drifts were removed from data before analysis, by convolving BOLD time series with a triangular filter kernel (48-s length) and subtracting the results from the time series. Analysis of the BOLD time series in each voxel begins with Fourier transform that decomposes the time series into the sum of Fourier components $A_0 \sin(2\pi f_0 t - \theta_0)$ at the stimulus repetition frequency (f_0 = 1/24 cycle/s) and $\sum_{f \neq f_0} A_f \sin(2\pi f t - \theta_f)$ at other frequencies, where A and θ are the amplitude and phase, respectively, of each Fourier component. The coherence level ρ, a value between 0 and 1, describes the relative significance of component at f_0 compared with other Fourier components

$$\rho = \frac{A_0}{\sqrt{A_0^2 + \sum_{f \neq f_0} A_f^2}}$$

In a blocked design where only two stimulus blocks are shown, the temporal phases of the two blocks differ by π radians. As a first-order approximation, the stimulus-driven component of BOLD response can be modeled as a sine wave with frequency f_0, and a phase value equal to the hemodynamic response delay φ if the response is stronger to the first block or $\pi + \varphi$ if the second (Logothetis and Wandell 2004). The amplitude of this stimulus-driven component is

$$\text{amplitude} = A_0 \cos(\theta_0 - \varphi)$$

The correlation coefficient describes how closely the BOLD response of each voxel fits this phase-specified sine wave model

$$r = \rho \cos(\theta_0 - \varphi)$$

r is a value between −1 and 1; strong positive values represent for significant strong responses to the first block, and negative values for the second block. Thus r denotes the statistical significance of stimulus-driven BOLD response (see Figs. 3 and 4).

The hemodynamic delay φ can be obtained from the standard hemodynamic response function (~3.5 s) (see Boynton et al. 1996) for all subjects. Alternatively, it can be estimated for each individual subject from the average θ_0 of strong BOLD responses to the "in-blank" and "out-blank" stimuli. We used the latter method and estimate φ to be close to 3.5 s for all three subjects. The amplitude and r are robust against small error in φ estimation because of their cosine relationships to φ.

TRAVELING-WAVE. In a traveling-wave design, positions across visual field are encoded into temporal phases of the stimulus, which in turn drives different BOLD response phases. The Fourier component $A_0 \sin(2\pi f_0 t - \theta_0)$ at stimulus repetition frequency f_0 comprises two parts: stimulus-driven BOLD signal with phase θ_{signal} and noise $A_{signal} \sin(2\pi f_0 t - \theta_{noise})$. To estimate θ_{signal}, we may hypothesize that the noise source has uniformly random phase θ_{noise} at f_0 and has a stationary frequency spectrum such that the noise power at f_0, A_{noise}^2, is directly proportional to power at other frequencies, $\sum_{f \neq f_0} A_f^2$. Predictions about the statistics of θ_0 can be made from these hypotheses when the noise is not too strong (coherence ρ is moderately large, e.g., >0.2). The SD of θ_0 is directly proportional to the noise-to-signal ratio (NSR) at f_0, which is $\sqrt{\sum_{f \neq f_0} A_f^2}/A_0 = \sqrt{1 - \rho^2}/\rho$. The distribution of θ_0 can be simulated, and is narrower than a Gaussian at high ρ. Both predictions are confirmed in measurements of phase variation in traveling-wave data (Fig. 8). The expectation value of the BOLD phase θ_0 at f_0 thus likely serves as a good estimate of θ_{signal}.

Next, the hemodynamic delay φ is subtracted from θ_{signal}, and the residual phase values correspond to the phase-encoded stimulus positions. Because we have traveling-wave data with pairs of stimuli time-reversed from each other (e.g., expanding and contracting rings), φ can be estimated from fitting the BOLD response phases of all retinotopic voxels to the relationship (Smith et al. 1998)

$$\theta_{expanding} + \theta_{contracting} = 2\varphi$$

This estimate of φ is very similar to estimate made in the previous (2-block) section.

In Fig. 2*A*, the eccentricity map is summarized from ring measurements of BOLD responses in gray matter and rendered as pseudo-

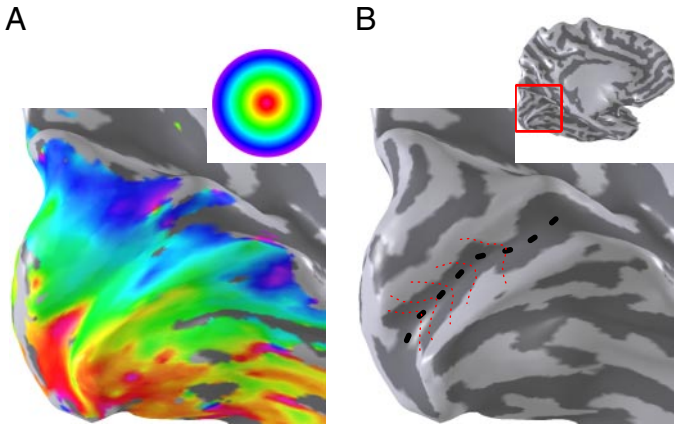

FIG. 2. Eccentricity map and V1 iso-eccentricity bands. *A*: eccentricity map representation shown on a smoothed representation of the cortical surface (gyrus: light shading; sulcus: dark shading). The pseudo-color map encodes the eccentricities eliciting maximum blood-oxygen-level-dependent (BOLD) response to an expanding ring stimulus (see *top right inset* for eccentricity legend). A clear eccentricity representation (central-to-peripheral) along the calcarine sulcus (posterior-to-anterior) is shown. *B*: on the same medial view of the cortical surface as *A* (see *inset* for relation to the whole brain), eccentricity increases along the calcarine sulcus (black dashed curve), and V1 can be subdivided into multiple iso-eccentricity bands (red dotted curves, all orthogonal to the black dashed curve). These bands are more compact near the posterior end, as consequence of cortical magnification. *Subject S1*.

color overlays on the smoothed cortical surface (boundary between gray and white matter). As seen from the medial view of visual cortex, the represented eccentricity is most central near the occipital pole, and becomes increasingly peripheral at more anterior locations along the calcarine sulcus (V1).

Amplitude profiles

To compute the distribution of BOLD responses in gray matter across the cortical surface, we can subdivide V1 into small regions equally spaced in cortical distance (Fig. 2*B*), each 1.5-mm wide and parallel to the iso-eccentricity direction (Dougherty et al. 2003). BOLD signals within each region were averaged and the average amplitude computed. The resulting amplitude profile is a function of the cortical distance in gray matter. This computation requires precise segmentation of the gray matter for accurate measurements of cortical distance. We manually edit the segmentation using mrGray software to ensure precision.

Alternatively, the amplitude results from fixed-aperture data and the eccentricity maps estimated from traveling wave stimuli were loaded together so that each voxel had the corresponding BOLD amplitude and eccentricity values. Voxels in V1 were then binned into multiple small regions; each region had eccentricity representation within a small range (1°). The distribution of BOLD amplitudes across these regions is the amplitude profile function of the eccentricity (e.g., Fig. 5). This computation is not significantly affected by the quality of gray matter segmentation and facilitates cross-subject averaging since the individual variances of cortical magnification are not included (Dougherty et al. 2003). On the other hand, it requires good spatial co-registration between the functional measurements and high-quality eccentricity maps (minimal noise in traveling wave data).

In principle, the two methods are equivalent, related through the cortical magnification relationship between eccentricity and cortical distance (Fig. 2*B*). By using two methods that are subject to different noise properties, we can quantitatively evaluate the change of amplitude profiles in units of eccentricity or cortical distance.

Analysis of Royal Holloway data

Data acquired at Royal Holloway were processed differently. Functional data were corrected for head motion (realign to the first volume), spatially smoothed [3-D Gaussian kernel; full width half-maximum (FWHM) of 2.5 mm for fixed-aperture and 5.0 mm for traveling wave data] and co-registered to the anatomical reference volume using FSL software (http://www.fmrib.ox.ac.uk/fsl/). Analysis was restricted to gray matter in the reference volume, segmented using mrGray. The fixed-aperture data were analyzed in SPM2 (http://www.fil.ion.ucl.ac.uk/spm/software/spm2/) assuming a standard hemodynamic response function. The data were high-pass temporal filtered (90-s cutoff). The SPM contrast was calculated by comparing the inward and outward blocks with blank blocks. The eccentricity and polar angle maps were estimated from the temporal phases of traveling-wave data using MedCon (http://xmedcon.sourceforge.net/) and our in-house software, with the hemodynamic delay cancelled using the aforementioned method (Smith et al. 1998). These visual field maps were mapped onto the flattened cortical surface as pseudo-color overlays, from which the boundaries of primary (V1), secondary (V2), and tertiary (V3) visual cortices were identified manually and regions of interest (ROIs) defined ≤35° eccentricity (Smith et al. 1998, 2001). Amplitude profiles were computed by loading the SPM contrast from fixed-aperture data and the visual field maps together.

RESULTS

We describe measurements of two groups of visual stimuli: fixed aperture and traveling wave. In the fixed-aperture measurements, stimuli presented at the same visual field position differed in motion direction (inward or outward). We created spatial profiles of the BOLD responses during the motion-direction exchange. In the traveling-wave experiments, we measured the temporal phases of BOLD responses to the traveling wave of stimulus positions and compared across conditions of different local motion direction.

Fixed-aperture measurements

REPLICATION OF RESULTS. The first experiment (in vs. out) compared cortical responses to stimuli in the same visual field position but moving in different directions. Subjects viewed a grating pattern within a ring aperture (7.5–13.5° eccentricity) that alternated between motion toward fixation (inward) or away from fixation (outward). This block alternation produced a periodic response in two distinct V1 regions: a relatively anterior region modulated in phase with inward motion (orange) and a relatively posterior region modulated in phase with outward motion (blue) (Fig. 3). The time series shows that the response amplitude was reliable but <0.5%.

These measurements replicate those described by Whitney et al. (2003). Specifically, alternating inward motion and outward motion produced BOLD modulations at two locations within V1 (in calcarine) separated by ~20 mm. Whitney et al. interpreted these responses as a flexible, stimulus-induced, reorganization of the visual field map (Fig. 2 in Whitney et al. 2003), so that the cortical region responding to stimuli in a fixed aperture changes depending on the stimulus motion. In the following, we perform a series of experiments to test this interpretation.

RETINOTOPIC REPRESENTATIONS ARE STABLE TO DIFFERENT STIMULUS MOTION. We performed an additional experiment using a block design in which the stimuli alternated between a moving

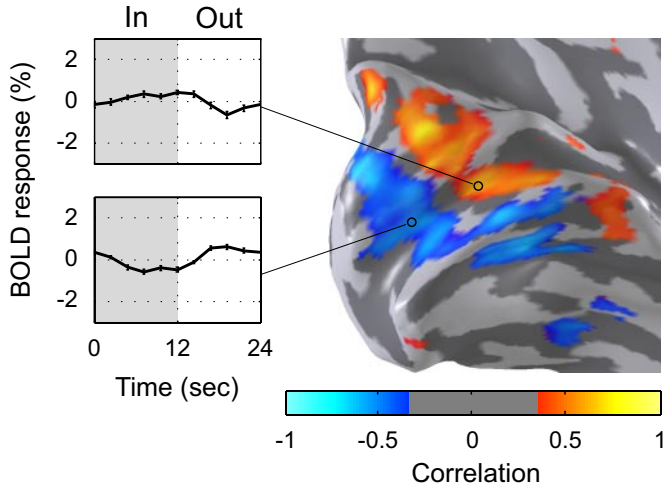

FIG. 3. BOLD signals in calcarine cortex during a motion-direction exchange experiment. A moving grating pattern was presented within a fixed aperture (see Fig. 1*A*). The grating alternated motion direction (inward or outward) every 12 s. This motion direction exchange produces weak but reliable BOLD responses in two widely separated calcarine regions. Maps of BOLD correlation with the stimulus are shown on the same cortical surface as in Fig. 2. The orange and blue regions have increased (positive) and decreased (negative correlation) BOLD responses, respectively, to the inward motion stimulus block. The time series show weak BOLD responses (~0.3%) in 2 locations within calcarine associated with the 2 directions of motion. A similar effect is evident in regions more remote from the calcarine, corresponding to V2/V3. *Subject S1.*

pattern and a uniform gray background (blank). We compared the spatial distribution of cortical responses for separate measurements made with inward (in vs. blank, Fig. 4*A*) and outward (out vs. blank, Fig. 4*B*) moving patterns. The stimuli were again presented within the same fixed aperture.

When measured under this design, the spatial distribution of cortical responses did *not* shift by 20 mm as stimulus motion changed (Fig. 4). Instead, the cortical regions overlap extensively independent of the direction of motion. The responsive cortical regions span a large surface area that includes the responsive regions in Fig. 3, and the time series modulation is about four times greater. Using this design, one concludes that the cortical region responding to the fixed aperture is approximately stable despite motion direction changes.

The responses to this moving pattern are robust in many retinotopic maps. The responses in Fig. 4 span V1, V2, V3 and hV4 (Fig. 4); activity was also present in MT+, V3A, V7, etc. (not shown). In V2, V3, and hV4, differential responses to motion direction like those in V1 are present (Fig. 3). However, it is worth noting that no subject showed reliable differential responses in MT+, the motion-selective cortex (data not shown). The representations in ventral higher-order areas (e.g., VO) are relatively weak, likely because the stimulus is relatively peripheral (Brewer et al. 2005).

QUANTITATIVE ANALYSIS OF THE LOCATION OF RESPONSIVE CORTICAL REGIONS. A quantitative examination of the data and additional experiments reveal why the flexible retinotopy interpretation is incorrect. We compare the two motion conditions by plotting the spatial distribution of the BOLD response amplitude in a series of V1 regions within different eccentricity bands (see METHODS). Figure 5 compares the response amplitudes between the three types of stimulus exchanges: in-out,

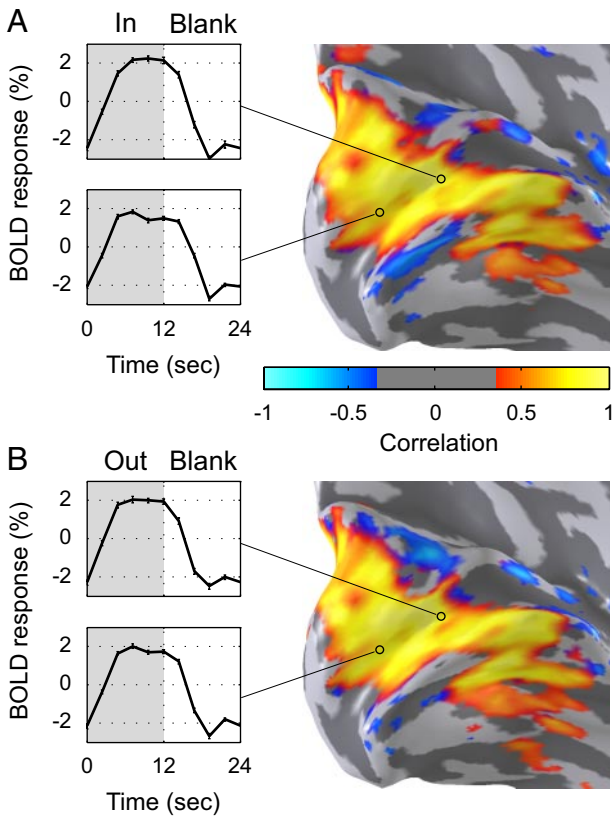

FIG. 4. BOLD signals in calcarine cortex during a stimulus-blank exchange. *A*: inward moving grating pattern within a fixed aperture, the same as the pattern used in Fig. 3, was alternated with a blank background. This in-blank exchange produces strong BOLD responses across the calcarine region and beyond, spanning ~1.5 cm in the posterior-anterior dimension. The responsive regions illustrated in Fig. 3 both fall within this responsive region. *B*: out-blank exchange produces a very similar pattern of BOLD responses, with no significant shift from that shown in *A*. The time series show strong BOLD responses (~2%) in the same regions as in Fig. 3. *Subject S1.*

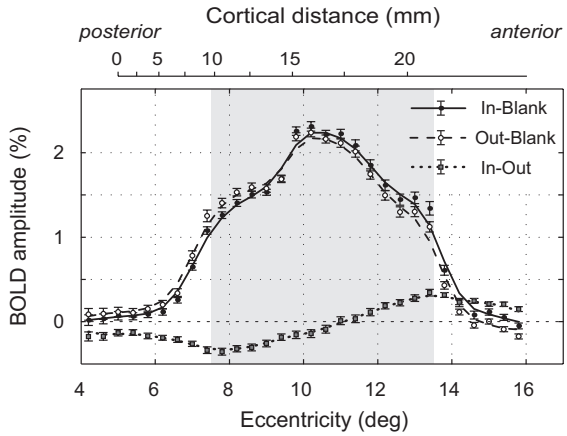

FIG. 5. Amplitude profile of BOLD responses. Response amplitudes were calculated for a series of bands representing a common eccentricity within V1. The band included voxels representing eccentricities falling within a 0.4° range. The responses to 3 types of stimulus exchanges are shown: in-blank (—), out-blank (- - -), and in-out (⋯). The lower horizontal axis measures the visual field eccentricity, and the upper horizontal axis measures the distance on the cortical surface with respect to the 5° representation. The shaded zone represents the stimulus aperture eccentricity range (7.5–13.5°). Smooth curves are drawn through the data. Error bar: ±1 SE. *Subject S1.*

in-blank, and out-blank. The amplitude profiles are plotted against cortical position along the calcarine sulcus.

The spatial locations of the in-blank and out-blank profiles differ little if at all. We quantify the locations of these profiles using two measures. First, we calculate the "center-of-mass" of the spatial distribution. This is the eccentricity weighted by the amplitude of each profile

$$\mathrm{CM}_{\mathrm{rec}} = \frac{\sum_{n}^{N} \mathrm{Amp}(n)\mathrm{Ecc}(n)}{\sum_{n}^{N} \mathrm{Amp}(n)}$$

where Amp(n) and Ecc(n) are, respectively, the BOLD amplitude and eccentricity of an eccentricity bin n, and N is the total number of bins. Similarly, the "center-of-mass" cortical distance ($\mathrm{CM}_{\mathrm{dist}}$) can be calculated across the cortical distance bins.

Second, we calculate spatial positions by fitting an asymmetric Gaussian function of eccentricity

$$\mathrm{Amp}(\mathrm{ecc}) = M \exp\left(-\left(\frac{\mathrm{ecc} - P_{\mathrm{ecc}}}{(1 + S_{\mathrm{ecc}}\mathrm{sgn}(\mathrm{ecc} - P_{\mathrm{ecc}}))\sigma} \right)^2 /2 \right)$$

where Amp is the BOLD amplitude, ecc is the eccentricity, M and σ are the fitting parameters, and sgn(x) is the sign function that is 1 when $x > 0$ and -1 when $x < 0$. The two parameters we calculate, P_{ecc} and S_{ecc}, describe the peak eccentricity and the skewness of the amplitude profile, respectively. Similarly, the peak P_{dist} and the skewness S_{dist} of the amplitude profile as function of cortical distance can be calculated.

By these quantitative measures, the amplitude profiles differ little between in-blank and out-blank measurements in each of the three Stanford subjects (1 of them, *S1,* is shown in Figs. 3–5). Table 1 shows the estimated $\mathrm{CM}_{\mathrm{dist}}$ and $\mathrm{CM}_{\mathrm{ecc}}$ differences for three individual subjects in V1. The differences in amplitude profiles are very small even when evaluated by the center-of-mass definition. The shift in $\mathrm{CM}_{\mathrm{ecc}}$ is ~0.5°, very small compared with the 7.5–13.5° eccentricity coverage of stimuli (Fig. 5). The peak P_{ecc} shift is not significant. The cortical distance shift $\mathrm{CM}_{\mathrm{dist}}$ is ~1 mm, which is small compared with the 2.5-mm voxel resolution.

The stability of amplitude profiles is further confirmed in Fig. 6, which combines the Royal Holloway data from six

TABLE 1. *Quantitative measures of amplitude profiles for subjects S1–S3*

Subject	*S1*	*S2*	*S3*
CM_{ecc}, °			
In	10.67 ± 0.14	10.24 ± 0.27	11.48 ± 0.09
Out	10.26 ± 0.18	9.48 ± 0.23	11.32 ± 0.13
Difference	0.41 ± 0.16	0.77 ± 0.30	0.16 ± 0.12
P_{ecc}, °			
In	10.57 ± 0.38	9.08 ± 0.50	10.69 ± 0.22
Out	10.53 ± 0.35	9.06 ± 0.64	10.63 ± 0.27
Difference	0.05 ± 0.35	0.02 ± 0.55	0.06 ± 0.24
CM_{dist}, mm			
In	13.93 ± 0.30	13.34 ± 0.47	15.75 ± 0.45
Out	12.73 ± 0.33	11.73 ± 0.54	15.20 ± 0.44
Difference	1.20 ± 0.31	1.61 ± 0.49	0.55 ± 0.48

Estimation of standard error is based on 500 resamples (with replacement) of the stimulus cycles. Data from *subject S1* are shown in Figs. 3–5. CM, center of mass.

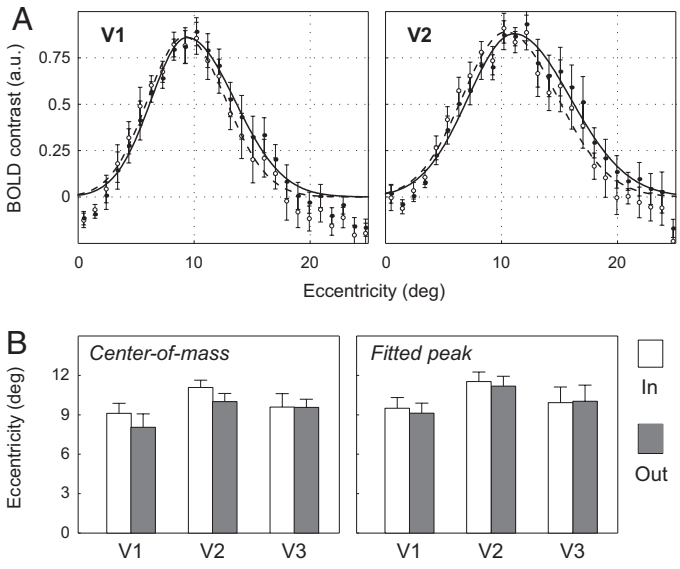

FIG. 6. Cross-subject spatial distribution of BOLD responses to inward and outward motion. *A*: BOLD response amplitudes and fitted asymmetric Gaussian curves for in-blank exchanges (●, —) and out-blank exchanges (○, - - -) in V1 and V2. *B*: eccentricities represented at the center-of-mass and at the peak BOLD response measured in V1, V2, and V3 (see text for details). The bars compare estimates from in-blank exchanges (□) and out-blank exchanges (▨). Error bars are ±1 SE across 12 hemispheres in 6 subjects (R1–R6).

subjects. The amplitude profiles in V1 and V2 (Fig. 6*A*), and V3 (not shown) between inward motion (●, —) and outward motion (○, - - -) have slight differences near the tails but not at the peaks of amplitude profiles. These differences are not significant at any eccentricity (note the error bars), and primarily skew the amplitude profiles and change the factor S_{ecc}. Consequently, the fitted peak P_{ecc} of amplitude profile does not change [$F(1,9) = 0.55$, $P > 0.5$ by 2-way repeated ANOVA], whereas the center-of-mass $\mathrm{CM}_{\mathrm{ecc}}$ is slightly shifted toward the central representation with outward motion, but this difference is not very significant [$F(1,9) = 0.62$, $P > 0.5$ by 2-way repeated ANOVA] (Fig. 6*B*). This group analysis across subjects suggests that the differential responses are not significant and arise primarily from the BOLD response near the edge of the stimulus representation.

We reached the same conclusion from measurements with a variety of other stimuli (data not shown). These include grating patterns that include the foveal field (aperture coverage: 0–13.5° eccentricity; otherwise the same parameters as in Stanford data), and small grating patterns (0–3° eccentricity) and Gabor patterns (in the Royal Holloway data, see METHODS).

MODELING THE SMALL RESPONSES TO MOTION DIRECTION DIFFERENCES. The BOLD response profile to the stimulus motion direction exchange (in vs. out) has a small, posterior trough (lower eccentricity) and a small, anterior peak (higher eccentricity). These local extremes are separated by ~1–2 cm and correspond to the negative ("blue") and positive ("orange") response regions in Fig. 3. Despite the seemingly large distance, both extremes are located within the neural representations of the "in" and "out" stimuli (Fig. 5), which are the responsive regions measured using the stimulus-blank exchanges (in vs. blank and out vs. blank). In this section, we examine whether very small differences between the responses to the two directions (when compared with blank) are sufficient

to cause the striking effect seen in Fig. 3, which, after all, reflects signals of very low amplitude. If they are, then (in a linear system) the difference between in-blank and out-blank should be equal to the differential response seen in the in-out exchange.

Figure 7*A* shows the amplitude difference between the neural representations of "in" and "out" stimuli computed from the mathematical subtraction between the BOLD responses to in-blank and out-blank exchanges (◇, —). The responses to motion direction exchange (in vs. out) are also shown for comparison (■, - - -). First, we note that the difference based on subtraction between neural representations is slightly weaker than the difference measured experimentally from the motion direction exchange.

We explain this failure of additivity as follows. In the block design of stimulus-blank exchange, the neural response alters between strong (to stimulus) and weak (to blank). The alternation amplitudes in the two similar exchanges (in vs. blank and out vs. blank) are similarly large. The small difference between the two large amplitudes is equal to the weak alternation amplitude of neural response in the motion direction exchange (in vs. out). In mathematical terms, we have

$$(I - B) \approx (O - B) \gg (I - O) = (I - B) - (O - B)$$

where I, O, and B denote the amplitude of neural response elicited by each of the three types of stimulus blocks (in, out, and blank), respectively.

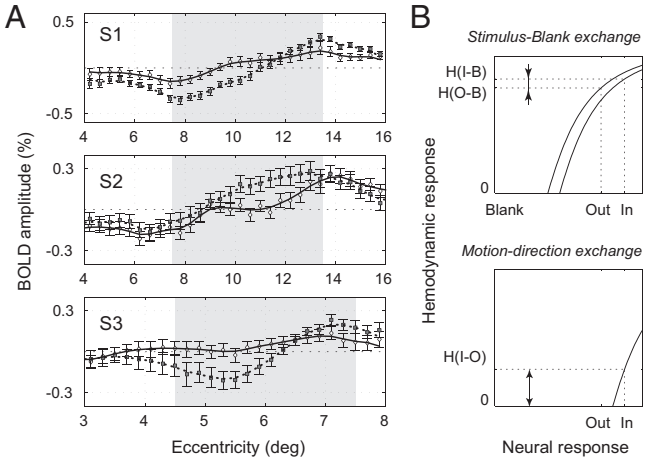

FIG. 7. Direct and indirect measures of the motion direction differences. *A*: response amplitudes to the direct exchange of motion direction (in-out; ■, - - -) are compared with the mathematical difference between (in-blank) and (out-blank) conditions (◇; —). The panels show measurements in 3 subjects (from top to bottom: *S1, S2, S3*). The shaded zone represents the stimulus aperture eccentricity range determined by visual field mapping. The pattern of responses from the direct measurements and the mathematical subtraction are similar, but the direct responses are slightly stronger than predicted by the subtraction. Error bar: ±1 SE. *B*: model illustration of why the in-out difference is suppressed in the indirect (mathematical subtraction) compared with the direct (in-out exchange) measure. Three neural activity levels corresponding to the 3 stimulus conditions (in, out, blank) are shown for an exemplar cortical region slightly more responsive to inward than outward motion. The hemodynamic response function, modeled as a compressive function of neural activity, is the same for each stimulus exchange, but centers (has zero amplitude) at the averaged neural response of each stimulus exchange [e.g., (in+blank)/2 for in-blank exchange]. The simulated BOLD amplitude *H* is much larger and more compressive during in-blank [*H*(I-B)]and out-blank [*H*(O-B)] exchanges (*top*) than during in-out exchange (*bottom*).

The BOLD amplitude is related to the neural response by the hemodynamic function H(). It is generally acceptable to model H() as a function with compressive nonlinearity (saturation) (for reviews, see Buxton et al. 2004; Logothetis and Wandell 2004). Figure 7*B* illustrates this model in a cortical region that is slightly more responsive to inward motion. The hemodynamic response is in a relatively linear range when the hemodynamic equilibrium is only weakly perturbed by the small alternation between two similar neural states, such as in the motion-direction exchange (*bottom*). On the other hand, in the stimulus-blank exchange (*top*) the neural response alternates significantly away from the baseline (blank) and drives the hemodynamic response to the nonlinear range, where the slope of response function is much shallower than in the linear range. As a consequence of the shallower slope, the same difference in neural responses may elicit smaller difference in hemodynamic responses. In mathematical terms, we have

$$H(I - B) - H(O - B) < H(I - O)$$

Thus the compressive nonlinearity predicts that the motion direction differences are best observed in BOLD responses through the direct alternation between two opposite motion directions (in vs. out).

Another finding from Fig. 7*A* is that although the difference between neural representations is small, the deviations are regular. Specifically, the subtraction-based difference (in vs. blank minus out vs. blank) is negative in the posterior (lower eccentricity) and positive in the anterior (higher eccentricity) regions; these regions are almost identical in location to the trough and peak of the response to in versus out. Both sets of data suggest that when the motion direction differs, the neural response difference is most robustly found in two separated cortical regions that correspond to the two tails of the spatial representation of the motion stimulus. This difference is also present in the group data (Fig. 6*B*) where the two amplitude profiles differ slightly in the two tails but not the peak.

Traveling wave measurements

To this point, visual field map stability was assessed using stimuli within a single visual field location. In the next set of experiments, we assessed the visual field map stability across different field positions. Specifically, we measured visual field eccentricity maps using conventional methods in which the stimulus is presented at a series of aperture positions. At each position the aperture contained a stimulus with either inward or outward motion (see METHODS). The purpose of the measurements was to quantify whether changes in the stimulus motion direction induces changes in the visual field map estimates.

First, we analyze the variance of repeated measurements made using the same stimulus. In traveling-wave experiments, the retinotopic position represented by each voxel is estimated from the temporal phase of the stimulus-driven component of the BOLD response. One phase value, θ_0, at the stimulus frequency (1 cycle/repetition) is estimated from each stimulus repetition (24 s). For each voxel in V1, the mean phase value θ_{scan} within a single scan (6 repetitions) is calculated. The within-scan phase difference values $\delta_{within} = \theta_0 - \theta_{scan}$ across all repetitions were pooled together and their distribution summarized in Fig. 8*A* ("within"). Each panel showed the distribution for V1 voxels around a certain level of coherence,

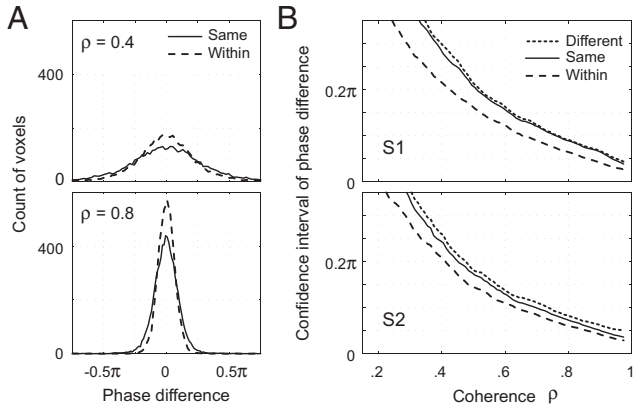

FIG. 8. Stability of the traveling-wave measurements. *A*: distribution of phases of BOLD V1 responses in each stimulus cycle of the traveling-wave experiment for the average phase within one scan ("within," - - -) or the average phase computed across scans of the same stimulus ("same," —). The distribution is approximately normal, and the variance is slightly larger for "same" than "within". The 2 panels show that the variance decreases with increasing coherence level. The top and bottom panels included V1 voxels within $\rho = 0.4 \pm 0.04$ and 0.8 ± 0.03, respectively. *Subject S1*. *B*: 68% confidence interval of the phase estimate decreases as a function of coherence level. At all coherence levels the confidence interval is smallest for within scan measurements ("within", - - -) and slightly higher when combining scans of the same motion direction ("same", —) or different directions ("different", · · ·). *Subjects S1* (*top*) and *S2* (*bottom*).

ρ, which was computed based on the averaged time series of scans with the same stimulus type. At a low coherence level ($\rho = 0.4$; *top*), δ_{within} distributes across a wide range. At a high coherence level ($\rho = 0.8$; *bottom*), the variance of δ_{within} is small and the distribution is well approximated by a normal curve.

Figure 8*B* characterizes the reliability of temporal phase measurements as a function of coherence level. The *top* and *bottom* show the 68%-confidence interval (half interval width) of the phase difference for *subjects S1* and *S2,* respectively. The interval is an estimate of the distribution width (SD if normal distribution) and hence the reliability of phase measurements. Within-scan interval is well-fit by a directly proportional relationship to the ratio $\sqrt{1 - \rho^2}/\rho$, supporting the model that noise is unrelated to the stimulus-driven BOLD signal (see METHODS). The accuracy of retinotopic measurements within a scan is highly similar for all three subjects (2 are shown). The 68%-confidence interval declines from $\sim 0.2\pi$ radians at $\rho \sim 0.4$ to 0.06π radians at $\rho \sim 0.8$. This interval multiplied by $24°/2\pi$ is the uncertainty of eccentricity measurements (stimuli had 1°/s eccentricity change, 24-s period).

Next, we analyzed the phase reliability in data from multiple scans performed using the same type of stimulus. We estimated the mean phase across all scans, θ_{same}, and computed the phase difference $\delta_{same} = \theta_0 - \theta_{same}$. The computation was done separately for the four types of stimuli, and the values were pooled together. The same-stimulus phase difference δ_{same} broadens when combining data across scans, compared with the within-scan phase spread (Fig. 8*A*) . The phase variation of δ_{same}, a combination of the repetition-to-repetition and the scan-to-scan noises, is ~20–30% greater than the variation of δ_{within} alone (Fig. 8*B*). This increase of confidence interval is also approximately proportional to $\sqrt{1 - \rho^2}/\rho$, suggesting that the spread is independent of the visual stimulus. Hence, the phase reliability degrades somewhat when pooling together scans separated by ≤1 h, possibly because of the slow instrumental drift and residual head movement despite motion correction. Our measurements of the repetition-to-repetition and scan-to-scan noises describe the limits of reliability of visual field map measurements in V1.

Finally, we examine the influence of stimulus motion direction on the map. If stimulus motion alters the visual field map, then pooling together inward and outward motion scans would significantly increase the phase confidence interval compared with that of same-stimulus δ_{same}. We estimated the mean phase combined across inward and outward motion scans, θ_{in+out}, and computed the phase difference $\delta_{different} = \theta_0 - \theta_{in+out}$. The computation was done separately for expanding ring and contracting ring stimuli, but the resultant phase difference values were pooled together. Comparing the across-motion-direction data ("different") to the same-stimulus data ("same", Fig. 8*B*), we find that combining the two types of stimulus motion direction does not change the phase confidence interval for *subjects S1* (Fig. 8*B, top*) and *S3* (not shown) and only increases slightly *for subject S2* (~0.015 π, equals to an eccentricity variance of 10 min of arc; see Fig. 8*B, bottom*). Hence, the phase reliability estimated without distinguishing motion direction ("different") differs insignificantly from that estimated with the distinction ("same"). The variance between opposite stimulus motion directions is thus much smaller than the inherent variance of visual field map measurements, indicating negligible influence of stimulus motion on visual field maps.

We also measured the phase reliability using ring stimuli that subtended 0–3° (Brewer et al. 2005). If the sources of phase noises are vision-related, e.g., because of excessive eye saccades, then the confidence interval (in units of radians) should increase with the smaller visual angle of ring stimuli. Instead, the phase confidence intervals ("within", "same", and "different") with the 3° ring stimuli (data not shown) are very similar to those measured with the 18° ring stimuli in Fig. 8. Thus the measured phase variances of visual field maps arise largely from instrumental and physiological noise and are uninfluenced by the visual stimulus.

DISCUSSION

In this paper, we tested the hypothesis that human V1 visual field map organization is dynamic, changing in response to stimulus motion direction. The experimental results that motivated the dynamic map (flexible retinotopy) hypothesis measured responses to inward and outward moving concentric stimuli (Whitney et al. 2003). We replicated these experiments (Fig. 3), but further experimental and analytical investigations do not support the flexible retinotopy hypothesis. Although the Stanford and Royal Holloway data differed significantly in methods of data acquisition and processing, we reached the same conclusions. Our measurements using the stimulus-blank exchanges (in-blank, out-blank) showed that visual field maps in V1 remain largely invariant to the stimulus motion direction. The neural representation changes in terms of the center-of-mass shift are even smaller than the spatial resolution of fMRI data (Figs. 4–6) and in terms of variances are smaller than the inherent variances in the traveling-wave measurements of visual field maps (Fig. 8). The seemingly dramatic shift in the locus of the neural representation of the stimulus (Fig. 3)

reflects a very modest change in the spatial distribution of responses. The possible origins of this change will be discussed in the following sections.

Modeling the small differences in receptive field properties

Whitney et al. (2003) favored a flexible retinotopy interpretation of the differential responses between opposite motions. Because receptive field size is the spatial limit of retinotopic encoding at the neuronal level, a meaningful flexibility requires the visual field map to change on a scale significantly larger than the neuronal receptive field size. At the eccentricities we probed, the receptive field size of an average neuron is ~0.8–1.5° in human V1 and a few times larger in V2 and V3 (Fu et al. 2004; Smith et al. 2001). Thus our estimates of the spatial changes of neural representations are only a fraction of the width of receptive field and *do not* support a flexible retinotopy interpretation.

On the other hand, small changes in receptive field response profiles may be the source of the differential responses to motion direction. To understand how the differences in the BOLD measurements could arise from these changes, we consider several models of how receptive field profiles might depend on stimulus motion. For this purpose, we describe a hypothetical single-unit electrophysiological experiment using a paradigm adapted from previous work (Berry et al. 1999; Fu et al. 2004).

Figure 9 illustrates the spatial response sensitivity of three hypothetical neurons with receptive fields contained within the aperture (gray vertical lines). The receptive fields are centered at the same visual field location. The *top three rows* show the three types of neurons, leftward-preferring, rightward-preferring and orthogonal. The graphs show the receptive field profile as a function of stimulus location in the visual field.

The three columns represent three different models of how receptive field spatial profiles depend on the stimulus motion. The spatial response profile to leftward and rightward motion is indicated by the — and - - -, respectively.

Figure 9, *left,* illustrates the "shift" model (Berry et al. 1999; Fu et al. 2004). In this model, stimulus motion direction dynamically re-weights the receptive fields of *all* responding neurons; the same re-weighting applies no matter what the neuron's directional selectivity is. The *middle panel* in the *left column* shows the re-weighting for a neuron preferring orthogonal motion. In the case of leftward motion, the spatial response profile increases in weight in the right half of the receptive field. This shifts the effective receptive field range, or the center of mass of the receptive field, in the direction opposite to the direction of motion. For a neuron selective to leftward motion (*top left*), the response is significantly stronger to leftward than to rightward motion, but the *normalized* spatial response profile re-weights with motion direction in the same way as other neurons in this model.

The average neural response profile is shown in the bottom row. Assuming that the center of mass of receptive field serves as the origin in neural computation of stimulus position, to match the effective receptive field shift against the stimulus motion direction, a moving stimulus would have to be perceived in a position ahead of its true position. The "shift" model thus explains the perceptual motion-induced shift (Fu et al. 2004). This model, however, fails to explain the fMRI results (Fig. 7), which show a shift in the opposite direction to that predicted by the model (Whitney et al. 2003).

Figure 9, *center*, illustrates the "reversed shift" model. This model shares all of its basic properties with the "shift" model but reverses the side of the receptive field that increases. This model explains the fMRI results; however, the motion-induced perceptual shift would then be unexplained. We note that even if we accept this basic model, the stimulus-induced receptive field shift measurements are only ~1/10 of receptive field size (Fu et al. 2004). These are too small compared with the shift required to explain the CM_{ecc} in our fMRI data [e.g., 0.5° or ~1/2 of receptive field size for human V1 (Smith et al. 2001)].

In Fig. 9, *right,* we propose a motion-direction asymmetry (MDA) model. In this model, the weights of spatial response

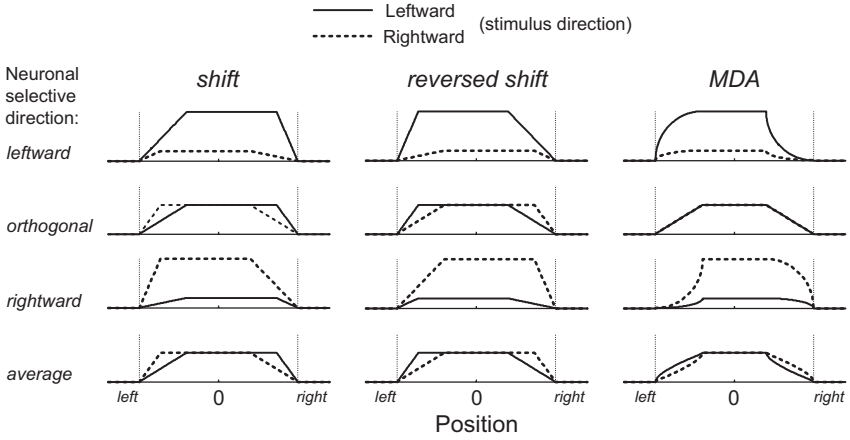

FIG. 9. Models of receptive field properties. We simulated neural response amplitudes as functions of the position (left-right) of a stationary aperture, within which grating patterns move leftward (—) or rightward (- - -). Position 0 is the center of the receptive field. As the stimulus is positioned at progressively more rightward locations, starting outside and to the left of the receptive field, the amplitude increases as the stimulus coverage increases until reaching a plateau where the stimulus fully covers the receptive field. At more rightward positions, the amplitude decreases with position from the plateau to baseline, as the stimulus coverage decreases. The figure shows simulated response profiles for 3 neurons (1st 3 rows) with directional tuning to leftward, orthogonal, and rightward motion (reflected by different plateau amplitudes), and the average neural response assuming that tuned directions distribute uniformly across neurons (4th row). Responses profiles are shown in 3 columns for 3 models [shift, reversed shift, and motion-direction asymmetry (MDA)] described in the text. The MDA model assumes that a direction-selective neuron has fixed asymmetry in stimulus responsivity along its preferred direction. The MDA model fits the fMRI data but does not entail any stimulus-related change in receptive field properties.

profiles do *not* change with stimulus motion; the weighting for each neuron depends on the neuron's directional selectivity. The spatial response profile of a neuron selective to leftward motion always responds more strongly (weights higher) in the left half than the right half of the receptive field, and conversely for a rightward selective neuron. Neurons selective to orthogonal motion direction have no asymmetry along the left-right axis. Such neuronal MDA could arise from stimulus-independent factors, such as asymmetry in density and/or strength of synapses within the receptive field. This model differs from the other two models because the asymmetry does not vary with the stimulus. The profile of averaged responses produced by these types of neurons shows a bias toward the left in case of leftward motion and to the right for rightward motion. Thus the MDA model, like the reversed shift model, explains the fMRI results but not the perceptual results. The MDA model does so without invoking any stimulus-induced change in the receptive field properties and is applicable to both hard and soft (Gabor) apertures regardless of the perceptual effect (Whitney et al. 2003). A relatively small asymmetry is sufficient to account for the differential BOLD responses to motion direction.

One key difference between the MDA and reversed shift model is in the predicted response to stimulus motion orthogonal to the preferred direction. The MDA model can be tested experimentally at the single-unit level by using stimuli much larger than the receptive field and jointly measuring the receptive field asymmetry and direction selectivity. To our knowledge such single-unit experiments have not been conducted (Fu et al. 2004; Livingstone 1998; Pack et al. 2003).

Optimal design to reveal subtle neural response differences

This paper employed two methods of BOLD imaging to reveal the subtle differences between neural responses to two similar stimuli. The first, direct method contrasts directly the two stimuli in a back-to-back block design ("in vs. out"). The measured BOLD responses relate directly to the neural response differences between the two stimulus conditions. The second, indirect method compares each of the two stimuli with the condition of no stimulus (blank screen) in the block design ("in vs. blank" or "out vs. blank"). In this method, the measured BOLD responses relate directly to the cortical neural representation of each stimulus; the response changes with motion direction are given indirectly by the difference between the two cortical representations.

Our data show clearly that the differential response is larger with the direct method, which can be explained through compressed nonlinearity between BOLD response and neural activity (Fig. 7). Such hemodynamic nonlinearity was found in joint recordings of BOLD response and local field potential in monkey visual cortex [Fig. 5D in Logothetis et al. (2001)] and in other experiments (Buxton et al. 2004). Based on this model, one may conclude that the direct method is the optimal experimental design to reveal subtle neural response differences due to changes in specific stimulus properties.

It appears appropriate to generalize this corollary to most neuroimaging experiments based on the neuro-hemodynamic coupling, where there is often no consensus on the optimal stimulus design. A good example is the fMRI measurements of orientation preference hyper-columns in V1. In early studies, two stimuli in different orientations were separated in time by a long presentation of blank screen or static stimuli, and responses of each stimulus in respect to blank were measured separately, equivalent to our indirect method described in the preceding text (Furmanski and Engel 2000; Kim et al. 2000). The later studies, aiming to improve the experimental design, presented continuously the stimuli in different orientations and observed directly the change of BOLD responses with the orientation, equivalent to our direct method (Sun et al. 2005; Wang et al. 2005).

The stimulus design employed by (Whitney et al. 2003) falls somewhere between direct and indirect methods. It was a random mixture of four types of stimulus blocks in an event-related design: two types of stimulus blocks with opposite motion direction (in and out) were mixed randomly with another two types of stimulus blocks (flickering and static). The in and out blocks could not be directly compared with each other in terms of BOLD response. Instead, their BOLD responses had to be calculated based on a baseline that corresponded to the average of the four blocks and had no clear physiological meaning. Furthermore, the retinotopic representations of "in" and "out" stimuli were not measured because the blank condition where no stimulus is present was not included.

A block design analyzing the subtraction of responses between two stimuli removes the common responses and amplifies the differences. To measure the similarity between the responses to the two stimuli, it is necessary to include other stimulus comparisons. In the case analyzed here, by adding measurements comparing moving stimuli and blank, as well as using the traveling-wave method that compares many stimuli, we find that V1 retinotopy is relatively stable to changes in the direction of stimulus motion.

ACKNOWLEDGMENTS

We thank S. Nakadomari, D. Ress, A. Wade, and D. Whitney for helpful discussions.

Present address of J. V. Liu: McGovern Institute, Massachusetts Institute of Technology, Cambridge, MA.

GRANTS

This study was partially supported by National Eye Institute Grant R01 EY-03164 to B. A. Wandell, the 21st century COE program (D-2 to Kyoto University), MEXT, Japan to H. Ashida, and The Wellcome Trust (UK) Grant GR070500 to A. T. Smith.

REFERENCES

Allman JM and Kaas JH. Representation of the visual field in striate and adjoining cortex of the owl monkey (*Aotus trivirgatus*). *Brain Res* 35: 89–106, 1971.

Ashida H and Smith AT. Retinotopic mapping of motion stimuli in human visual cortex. *Vision Sci Soc Abstr* 5, 489a, 2005.

Berry MJ, II, Brivanlou IH, Jordan TA, and Meister M. Anticipation of moving stimuli by the retina. *Nature* 398: 334–338, 1999.

Boynton GM, Engel SA, Glover GH, and Heeger DJ. Linear systems analysis of functional magnetic resonance imaging in human V1. *J Neurosci* 16: 4207–4221, 1996.

Brewer AA, Press WA, Logothetis NK, and Wandell BA. Visual areas in macaque cortex measured using functional magnetic resonance imaging. *J Neurosci* 22: 10416–10426, 2002.

Brewer AA, Liu J, Wade AR, and Wandell BA. Visual field maps and stimulus selectivity in human ventral occipital cortex. *Nat Neurosci* 8: 1102–1109, 2005.

Buxton RB, Uludag K, Dubowitz DJ, and Liu TT. Modeling the hemodynamic response to brain activation. *Neuroimage* 23:S220–S233, 2004.

Darian-Smith C and Gilbert CD. Topographic reorganization in the striate cortex of the adult cat and monkey is cortically mediated. *J Neurosci* 15: 1631–1647, 1995.

DeYoe EA, Carman GJ, Bandettini P, Glickman S, Wieser J, Cox R, Miller D, and Neitz J. Mapping striate and extrastriate visual areas in human cerebral cortex. *Proc Natl Acad Sci USA* 93: 2382–2386, 1996.

Dougherty RF, Koch VM, Brewer AA, Fischer B, Modersitzki J, and Wandell BA. Visual field representations and locations of visual areas V1/2/3 in human visual cortex. *J Vis* 3: 586–598, 2003.

Engel SA, Glover GH, and Wandell BA. Retinotopic organization in human visual cortex and the spatial precision of functional MRI. *Cereb Cortex* 7: 181–192, 1997.

Engel SA, Rumelhart DE, Wandell BA, Lee AT, Glover GH, Chichilnisky EJ, and Shadlen MN. fMRI of human visual cortex (Letter) [published erratum appears in *Nature* 370: 106, 1994]. *Nature* 369: 525, 1994.

Fu YX, Shen Y, and Dan Y. Motion-induced perceptual extrapolation of blurred visual targets (Rapid Communication). *J Neurosci* 21: RC172, 2001.

Fu YX, Shen Y, Gao H, and Dan Y. Asymmetry in visual cortical circuits underlying motion-induced perceptual mislocalization. *J Neurosci* 24: 2165–2171, 2004.

Furmanski CS and Engel SA. An oblique effect in human primary visual cortex. *Nat Neurosci* 3: 535–536, 2000.

Gilbert CD. Adult cortical dynamics. *Physiol Rev* 78: 467–485, 1998.

Gilbert CD and Wiesel TN. Receptive field dynamics in adult primary visual cortex. *Nature* 356: 150–152, 1992.

Griswold MA, Jakob PM, Heidemann RM, Nittka M, Jellus V, Wang J, Kiefer B, and Haase A. Generalized autocalibrating partially parallel acquisitions (GRAPPA). *Magn Reson Med* 47: 1202–1210, 2002.

Horton JC and Hocking DR. Monocular core zones and binocular border strips in primate striate cortex revealed by the contrasting effects of enucleation, eyelid suture, and retinal laser lesions on cytochrome oxidase activity. *J Neurosci* 18: 5433–5455, 1998.

Kaas J. Theories of visual cortex organisation in primates. *Cereb Cortex* 12: 91–125, 1997a.

Kaas JH. Topographic maps are fundamental to sensory processing. *Brain Res Bull* 44: 107–112, 1997b.

Kim DS, Duong TQ, and Kim SG. High-resolution mapping of iso-orientation columns by fMRI. *Nat Neurosci* 3: 164–169, 2000.

Liu J, Ress D, Nakadomari S, and Wandell BA. Stability of human V1 retinotopy measured with moving patterns. *Soc Neurosci Abstr* 18.11, 2004.

Liu J and Wandell BA. Specializations for chromatic and temporal signals in human visual cortex. *J Neurosci* 25: 3459–3468, 2005.

Livingstone MS. Mechanisms of direction selectivity in macaque V1. *Neuron* 20: 509–526, 1998.

Logothetis NK, Pauls J, Augath M, Trinath T, and Oeltermann A. Neurophysiological investigation of the basis of the fMRI signal. *Nature* 412: 150–157, 2001.

Logothetis NK and Wandell BA. Interpreting the BOLD signal. *Annu Rev Physiol* 66: 735–769, 2004.

Nestares O and Heeger DJ. Robust multiresolution alignment of MRI brain volumes. *Magn Reson Med* 43: 705–715, 2000.

Pack CC, Livingstone MS, Duffy KR, and Born RT. End-stopping and the aperture problem: two-dimensional motion signals in macaque V1. *Neuron* 39: 671–680, 2003.

Rosa MG, Schmid LM, and Calford MB. Responsiveness of cat area 17 after monocular inactivation: limitation of topographic plasticity in adult cortex. *J Physiol* 482: 589–608, 1995.

Sereno MI, Dale AM, Reppas JB, Kwong KK, Belliveau JW, Brady TJ, Rosen BR, and Tootell RB. Borders of multiple visual areas in humans revealed by functional magnetic resonance imaging. *Science* 268: 889–893, 1995.

Smirnakis SM, Brewer AA, Schmid MC, Tolias AS, Schüz A, Augath M, Inhoffen W, Wandell BA, and Logothetis NK. Adult macaque V1 fails to reorganize in the months following homonymous retinal lesions. *Nature* 435: 300–305, 2005.

Smith AT, Greenlee MW, Singh KD, Kraemer FM, and Hennig J. The processing of first- and second-order motion in human visual cortex assessed by functional magnetic resonance imaging (fMRI). *J Neurosci* 18: 3816–3830, 1998.

Smith AT, Singh KD, Williams AL, and Greenlee MW. Estimating receptive field size from fMRI data in human striate and extrastriate visual cortex. *Cereb Cortex* 11: 1182–1190, 2001.

Sun P, Gardner J, Costagli M, Ueno K, Tanaka K, and Cheng K. Direct demonstration of tuning to stimulus orientation in human V1: a high-resolution fMRI study with a novel stimulation paradigm. *Soc Neurosci Abstr* 618.9, 2005.

Wandell BA, Brewer AA, and Dougherty RF. Visual field map clusters in human cortex. *Philos Trans R Soc Lond B Biol Sci* 360: 693–707, 2005.

Wang P, Moon C, Fukuda H, and Kim S. Evaluation of iso-orientation maps in cat visual cortex revealed by functional MRI. *Soc Neurosci Abstr* 508.5, 2005.

Whitney D, Goltz HC, Thomas CG, Gati JS, Menon RS, and Goodale MA. Flexible retinotopy: motion-dependent position coding in the visual cortex. *Science* 302: 878–881, 2003.